INTERNATIONAL JOURNAL FOR NUMERICAL METHODS IN ENGINEERING
Int. J. Numer. Meth. Engng (2008)
Published online in Wiley InterScience (www.interscience.wiley.com). DOI: 10.1002/nme.2510

A multiscale framework for computational nanomechanics: Application to the modeling of carbon nanotubes

Arif Masud[1,*,†,‡] and Raguraman Kannan[2,§]

[1]*Department of Civil and Environmental Engineering, University of Illinois at Urbana-Champaign, Urbana, IL 61801, U.S.A.*
[2]*Department of Civil and Materials Engineering, University of Illinois at Chicago, Chicago, IL 60607, U.S.A.*

SUMMARY

A multiscale computational framework is presented that provides a coupled self-consistent system of equations involving molecular mechanics at small scales and quasi-continuum mechanics at large scales. The proposed method permits simultaneous resolution of quasi-continuum and atomistic length scales and the associated displacement fields in a unified manner. Interatomic interactions are incorporated into the method through a set of analytical equations that contain nanoscale-based material moduli. These material moduli are defined via internal variables that are functions of the local atomic configuration parameters. Point defects like vacancy defects in nanomaterials perturb the atomic structure locally and generate localized force fields. Formation energy of vacancy is evaluated via interatomic potentials and minimization of this energy leads to nanoscale force fields around defects. These nanoscale force fields are then employed in the multiscale method to solve for the localized displacement fields in the vicinity of vacancies and defects. The finite element method that is developed based on the hierarchical multiscale framework furnishes a two-level statement of the problem. It concurrently feeds information at the molecular scale, formulated in terms of the nanoscale material moduli, into the quasi-continuum equations. Representative numerical examples are shown to validate the model and demonstrate its range of applicability. Copyright © 2008 John Wiley & Sons, Ltd.

Received 6 August 2008; Accepted 15 October 2008

KEY WORDS: multiscale formulation; bridging scales; carbon nanotubes; molecular mechanics; vacancy defects; finite element analysis; interatomic potentials; graphene sheets

*Correspondence to: Arif Masud, Department of Civil and Environmental Engineering, University of Illinois at Urbana-Champaign, Urbana, IL 61801, U.S.A.
†E-mail: amasud@illinois.edu
‡Associate Professor.
§Graduate Research Assistant.

Contract/grant sponsor: Office of Naval Research; contract/grant number: N000014-02-1-0143
Contract/grant sponsor: National Academy of Sciences; contract/grant number: NAS 7251-05-005

1. INTRODUCTION

Carbon nanotubes (CNTs) are cylindrical structures composed of carbon atoms in a periodic hexagonal arrangement. From a nanostructure viewpoint CNTs can be regarded as graphene sheets, i.e. 2-D array of carbon atoms in a hexagonal pattern, rolled up in a way as to form seamless cylinders [1]. Nanotubes possess remarkable mechanical and electronic properties that make them promising candidates for application in nanotechnology [2, 3]. Modeling of these nanomaterials involves phenomena with multiple spatial and temporal scales and this has attracted considerable attention from the research community. In general, two approaches have been adopted by various researchers to describe material properties at small and large length scales: (i) the 'bottom up' approach that is based on quantum/molecular mechanics and (ii) the 'top down' approach that is based on continuum mechanics. A good account of the modeling issues in CNTs and an overview of the various methods proposed in the literature is presented in Liu and coworkers [4, 5], Belytschko *et al*. [6–8], Yakobson and coworkers [9, 10], and references therein.

The availability of accurate interatomic potentials makes classical MD simulations a prominent tool for modeling nanotubes [11–15]. However, single scale methods such as '*ab initio*' quantum mechanics methods or molecular dynamics (MD) methods have difficulty in analyzing hybrid structures due to the limitations in terms of the time and the length scales that these methods are confined to [5, 7]. Qian *et al*. [4] indicate that despite the increase in the computational power and improvement in algorithms, classical MD simulation is limited to 10^6–10^8 atoms for a few nanoseconds. On the other hand, pure continuum-based models for nanomechanics are not sensitive to the changes in the local atomic configurations and, therefore, cannot account for the nanoscale effects. One numerical approach that has been applied to many problems is to use MD only in localized regions in which the atomic-scale dynamics are important, while using a continuum simulation method everywhere else [7, 16–18]. The issue of disparate time scales in the two regions has been addressed and some simplified treatments of the interface between the atomistic and continuum regimes have been proposed [5]. Zhang and coworkers have proposed a nanoscale-based continuum theory [19, 20], and Chang and Gao have developed stick-spiral models for CNTs and graphene sheet [21].

In the present era of nanotechnology, it has become increasingly important to model phenomena at microscopic length scales that lie between the mesoscopic scales and the nanoscales. However a microscopic model can involve up to a scale of several microns consisting of billions of atoms, which is outside the range of MD simulations to date [4]. In view of these technical difficulties, new multiscale approaches are required to successfully address the class of problems where molecular scales interact with microscales [22]. For some successful multiscale approaches that provide a link between quantum/molecular and continuum descriptions of the material properties, the interested reader is referred to the works of Belytschko and Xiao [7], Liu and coworkers [4, 5], and Huang and coworkers [23] (and references therein).

This paper presents a mathematically consistent multiscale computational framework for bridging the gap between molecular mechanics and qausi-continuum mechanics in the modeling of CNTs. Contrary to the 'computational' nesting of information from smaller scales into the larger ones, we propose a novel mathematical nesting of scales that yields the hierarchical multiscale method. We employ two overlapping domains: a quasi-continuum domain for the defect-free graphene sheets and nanotubes and an atomistic domain that overlays the region containing point defects and models the localized fields around defects. For the modeling of the quasi-continuum domain, interatomic potentials [11, 15] are incorporated in the stick-spiral model of Chang and Gao [21]

DOI: 10.1002/nme

that yields nanoscale-based mechanical material moduli via a set of analytical equations. These material moduli are functions of internal variables of changes in bond lengths and bond angles, and are then used in the quasi-continuum modeling of the defect-free nanostructures. In the atomistic calculations around the point defects, the formation energy of vacancy (Section 4.1) [24, 25] is evaluated and employed in conjunction with the stick-spiral model [21] to account for the local changes in the atomic structure and to generate the localized force fields. These localized nanoscale force fields are then used in the variational multiscale method to model the localized displacements in the vicinity of vacancies and defects.

An outline of the paper is as follows. In Section 2 we present the general variational multiscale framework that underlies the proposed computational nanomechanics method. Section 3 presents the stick-spiral molecular mechanics model [21] embedded with interatomic potentials [11, 15] to extract scale-dependent material properties of continuously deforming CNTs. Section 4 presents the formation energy of vacancy that is employed to extract the localized material properties in the vicinity of the defects, and a method to extract the driving forces for the modeling of mechanical fields around the point defects. Numerical results are presented in Section 5 and conclusions are drawn in Section 6.

2. A MULTISCALE COMPUTATIONAL FRAMEWORK

This section presents a mathematically consistent multiscale framework for bridging the gap between molecular mechanics at the very fine-scales and quasi-continuum mechanics at the microscales in the modeling of micro- and nanostructures. Employing the hierarchical multiscale variational framework presented in Masud *et al*. [26, 27] and Masud and Franca [28] we illustrate the key ideas underlying the proposed multiscale method for computational micro- and nanomechanics.

2.1. Two-level scale separation

Let $\Omega \subset \mathbb{R}^{n_{\text{sd}}}$ be an open bounded region with piecewise smooth boundary Γ. In general the number of space dimensions n_{sd} is equal to 3, however, for planar nanomaterials like graphene sheets or unwrapped nanotubes, n_{sd} is equal to 2. Boundary Γ admits a unique decomposition $\Gamma = \Gamma_g \cup \Gamma_h$, where Γ_g and Γ_h are parts of the boundary with prescribed Dirichlet and Neumann conditions, respectively. Let $\mathscr{L}$ be the operator of the equation governing the deformation of the nanostructure. Abstract form of the governing equation is:

$$\mathscr{L}\mathbf{u} = \mathbf{f} \quad \text{in } \Omega \tag{1}$$

where $\mathbf{u}$ is the unknown field and $\mathbf{f}$ is the forcing function. Without loss of generality we consider Dirichlet-type boundary conditions $\mathbf{u} = \mathbf{g}$ on Γ_g. The standard variational form can be expressed as

$$(\mathbf{w}, \mathscr{L}\mathbf{u}) = (\mathbf{w}, \mathbf{f}) \tag{2}$$

where $\mathbf{w}$ represents the appropriate test functions and $(\cdot,\cdot) = \int_\Omega (\cdot)\, \mathrm{d}\Omega$ is the $L_2(\Omega)$-inner product. We consider discretization of the domain into non-overlapping subregions/elements. The sum over the interiors of these subregions is indicated as Ω' and is defined as $\Omega' = \bigcup_{e=1}^{n_{\text{umel}}} (\text{int})\Omega^e$, where n_{umel} is the total number of elements in the computational grid. The sum over element boundaries is indicated as Γ' and is defined as $\Gamma' = \bigcup_{e=1}^{n_{\text{umel}}} \Gamma^e$.

DOI: 10.1002/nme

We assume an overlapping additive decomposition of the total solution into coarse-scales $\tilde{\mathbf{u}}$ (i.e. meso-to-microscales) and fine-scales $\mathbf{u}'$ (i.e. micro-to nanoscales), represented as

$$\mathbf{u} = \tilde{\mathbf{u}} + \mathbf{u}' \tag{3}$$

Likewise we assume an overlapping sum decomposition of the weighting function

$$\mathbf{w} = \tilde{\mathbf{w}} + \mathbf{w}' \tag{4}$$

where $\tilde{\mathbf{w}}$ are the weighting functions for the coarse scales and $\mathbf{w}'$ are the weighting functions for the fine scales. To keep the presentation simple and without loss of generality, we assume that the fine scales vanish at the inter-element boundaries Γ'.

We also assume a unique additive decomposition of the forcing function into coarse-scales $\tilde{\mathbf{f}}$ (meso-to-micro) and fine-scales $\mathbf{f}'$ (micro-to-nano) components, represented as

$$\mathbf{f} = \tilde{\mathbf{f}} + \mathbf{f}' \tag{5}$$

Substituting the additively decomposed $\mathbf{u}$, $\mathbf{w}$ and $\mathbf{f}$ in (2) we get

$$(\tilde{\mathbf{w}} + \mathbf{w}', \mathscr{L}(\tilde{\mathbf{u}} + \mathbf{u}')) = (\tilde{\mathbf{w}} + \mathbf{w}', \tilde{\mathbf{f}} + \mathbf{f}') \tag{6}$$

The proposed decomposition of the forcing function gives rise to a further decomposition of the coarse and fine-scale solutions such that

$$\tilde{\mathbf{u}} = \tilde{\mathbf{u}}_{\tilde{\mathbf{f}}} + \tilde{\mathbf{u}}_{\mathbf{f}'} \tag{7}$$

$$\mathbf{u}' = \mathbf{u}'_{\tilde{\mathbf{f}}} + \mathbf{u}'_{\mathbf{f}'} \tag{8}$$

wherein $\tilde{\mathbf{u}}_{\tilde{\mathbf{f}}}$ and $\mathbf{u}'_{\tilde{\mathbf{f}}}$ are the coarse and fine-scale components of the solution that arise because of meso-to-micro force terms $\tilde{\mathbf{f}}$. Similarly, $\tilde{\mathbf{u}}_{\mathbf{f}'}$ and $\mathbf{u}'_{\mathbf{f}'}$ are the coarse and fine-scale components of the solution that arise because of micro-to-nano force terms $\mathbf{f}'$. Substituting (7) and (8) in (6) we get

$$(\tilde{\mathbf{w}} + \mathbf{w}', \mathscr{L}((\tilde{\mathbf{u}}_{\tilde{\mathbf{f}}} + \tilde{\mathbf{u}}_{\mathbf{f}'}) + (\mathbf{u}'_{\tilde{\mathbf{f}}} + \mathbf{u}'_{\mathbf{f}'}))) = (\tilde{\mathbf{w}} + \mathbf{w}', \tilde{\mathbf{f}} + \mathbf{f}') \tag{9}$$

Equation (9) yields a fully coupled system for the coarse and fine solution fields that arise because of the meso–micro forcing functions $\tilde{\mathbf{f}}$ and the micro–nano forcing functions $\mathbf{f}'$. Assuming a unique additive decomposition of $\mathbf{f}$ into $\tilde{\mathbf{f}}$ and $\mathbf{f}'$, we can split (9) into two subproblems.

Meso–Micro Scale Problem:

$$(\tilde{\mathbf{w}} + \mathbf{w}', \mathscr{L}(\tilde{\mathbf{u}}_{\tilde{\mathbf{f}}} + \mathbf{u}'_{\tilde{\mathbf{f}}})) = (\tilde{\mathbf{w}} + \mathbf{w}', \tilde{\mathbf{f}}) \tag{10}$$

Micro–Nano Scale Problem:

$$(\tilde{\mathbf{w}} + \mathbf{w}', \mathscr{L}(\tilde{\mathbf{u}}_{\mathbf{f}'} + \mathbf{u}'_{\mathbf{f}'})) = (\tilde{\mathbf{w}} + \mathbf{w}', \mathbf{f}') \tag{11}$$

Remark 1

In this framework $\tilde{\mathbf{f}}$ represents the quasi-continuum forcing functions while $\mathbf{f}'$ represents the point forces associated with the point defects. These point forces are obtained via inter-atomic potentials as explained in Section 4.

DOI: 10.1002/nme

Remark 2
The mathematical conditions on the split of (9) into (10) and (11) for the case where the underlying Equation (1) is non-linear are discussed in Masud and Franca [28].

It is important to note that if we sum (10) and (11), we recover Equation (9). Equation (10) is driven by the meso-to-micro force terms $\tilde{\mathbf{f}}$ and it yields solution fields $\tilde{\mathbf{u}}_{\tilde{\mathbf{f}}}$ and $\mathbf{u}'_{\tilde{\mathbf{f}}}$. Likewise, Equation (11) is driven by micro-to-nano force terms $\mathbf{f}'$ and it yields the solution fields $\tilde{\mathbf{u}}_{\mathbf{f}'}$ and $\mathbf{u}'_{\mathbf{f}'}$ that are meso-to-micro and micro-to-nano fields, respectively. We now split the *meso–microscale problem* and the *micro–nanoscale problem* into sub-system 1 and sub-system 2, respectively.

Sub-system 1: Employing the linearity of the weighting function slot in (10) and (11) we get the following two problems for the coarse or the meso-to-microscales:

$$(\tilde{\mathbf{w}}, \mathscr{L}(\tilde{\mathbf{u}}_{\tilde{\mathbf{f}}} + \mathbf{u}'_{\tilde{\mathbf{f}}})) = (\tilde{\mathbf{w}}, \tilde{\mathbf{f}}) \tag{12}$$

$$(\tilde{\mathbf{w}}, \mathscr{L}(\tilde{\mathbf{u}}_{\mathbf{f}'} + \mathbf{u}'_{\mathbf{f}'})) = (\tilde{\mathbf{w}}, \mathbf{f}') \tag{13}$$

Sub-system 2: Similarly, from (10) and (11) we get two problems for the fine or the micro-to-nano scales:

$$(\mathbf{w}', \mathscr{L}(\tilde{\mathbf{u}}_{\tilde{\mathbf{f}}} + \mathbf{u}'_{\tilde{\mathbf{f}}})) = (\mathbf{w}', \tilde{\mathbf{f}}) \tag{14}$$

$$(\mathbf{w}', \mathscr{L}(\tilde{\mathbf{u}}_{\mathbf{f}'} + \mathbf{u}'_{\mathbf{f}'})) = (\mathbf{w}', \mathbf{f}') \tag{15}$$

The key idea at this point is to solve the sub-system 2 locally so as to extract the fine-scale solution components $\mathbf{u}'_{\tilde{\mathbf{f}}}$ and $\mathbf{u}'_{\mathbf{f}'}$. These components can then be substituted in the sub-system 1, thereby eliminating the fine scales, yet retaining their effects. As presented in Masud and Franca [28], the solution of (14) when substituted in (12) leads to the following multiscale form of the variational problem where the fine-scale solution induced by the fine-scale forcing function is mathematically embedded in the corresponding coarse-scale problem.

$$(\tilde{\mathbf{w}}, \mathscr{L}\tilde{\mathbf{u}}_{\tilde{\mathbf{f}}}) + (\mathscr{L}^*\tilde{\mathbf{w}}, -\tau_1 \mathscr{L}\tilde{\mathbf{u}}_{\tilde{\mathbf{f}}}) = (\tilde{\mathbf{w}}, \tilde{\mathbf{f}}) - (\mathscr{L}^*\tilde{\mathbf{w}}, \tau_1\tilde{\mathbf{f}}) \tag{16}$$

where $\mathscr{L}^*$ is the adjoint operator. The boundary term is annihilated due to the assumption of fine-scales becoming zero at the inter-element boundaries, i.e. $\mathbf{u}'_{\tilde{\mathbf{f}}} = \mathbf{0}$ on Γ'. The second term on the left-hand side in (16) is the multiscale/stabilization term and is a function of the residual of the resolvable scales, i.e. function of the residual of coarse scales. Consequently, Equation (16) gives rise to a stabilized form for the subproblem, which is driven by the meso-to-micro force terms $\tilde{\mathbf{f}}$, and it will be used to model the defect-free nanostructures.

Likewise we can take Equation (15), which is the fine-scale problem driven by the fine-scale forcing functions and extract $\mathbf{u}'_{\mathbf{f}'}$ via analytical or numerical methods. The functional form of $\mathbf{u}'_{\mathbf{f}'}$ can then be substituted in the corresponding coarse-scale problem given by Equation (13). This results in the following variational form that is driven by the micro-to-nano force terms $\mathbf{f}'$, and it will be used to model the fine-scale fields around the defects in nanostructures:

$$(\tilde{\mathbf{w}}, \mathscr{L}\tilde{\mathbf{u}}_{\mathbf{f}'}) + (\mathscr{L}^*\tilde{\mathbf{w}}, -\tau_2 \mathscr{L}\tilde{\mathbf{u}}_{\mathbf{f}'}) = (\tilde{\mathbf{w}}, \mathbf{f}') - (\mathscr{L}^*\tilde{\mathbf{w}}, \tau_2\mathbf{f}') \tag{17}$$

It is important to realize that the solution of (17) gives $\tilde{\mathbf{u}}_{\mathbf{f}'}$ which is the coarse-scale component of the solution field that arises because of the micro-to-nano force terms $\mathbf{f}'$.

DOI: 10.1002/nme

Remark 3
Equations (16) and (17) present a system of two equations that yield the scale-dependent solutions to the governing equation that is driven by scale-dependent forcing functions, respectively.

Remark 4
The proposed method provides a framework for bridging the scales in computational micro and nanomechanics. In this context $\mathbf{u}'_{\tilde{\mathbf{f}}}$ and $\tilde{\mathbf{u}}_{\mathbf{f}'}$ are the bridging scales as they transfer information from one scale level to the other.

2.2. Significant aspects of the multiscale framework

This section summarizes the important aspects of the proposed framework for computational micro- and nanomechanics.

1. From (14) we obtain $\mathbf{u}'_{\tilde{\mathbf{f}}}$, which when substituted in (12) gives rise to the variational equation (16) that yields a multiscale/stabilized form for $\tilde{\mathbf{u}}_{\tilde{\mathbf{f}}}$. This equation furnishes the solution $\tilde{\mathbf{u}}_{\tilde{\mathbf{f}}}$ where the effects of the bridging scale $\mathbf{u}'_{\tilde{\mathbf{f}}}$ that arises because of meso-to-micro force terms $\tilde{\mathbf{f}}$ are mathematically embedded.
2. From (15) we obtain $\mathbf{u}'_{\mathbf{f}'}$ which is the fine-scale solution induced by the fine-scale forcing functions. Substituting $\mathbf{u}'_{\mathbf{f}'}$ in (13) gives rise to a multiscale/stabilized form for $\tilde{\mathbf{u}}_{\mathbf{f}'}$. This component of the unknown field arises because of micro-to-nano force terms $\mathbf{f}'$, and plays the role of bridging scales in our framework.
3. The total solution to the problem is obtained via the principal of superposition.

$$\tilde{\mathbf{u}} = \tilde{\mathbf{u}}_{\tilde{\mathbf{f}}} + \tilde{\mathbf{u}}_{\mathbf{f}'} \tag{18}$$

   For the case of non-linear problems one can employ the Lagrange multiplier method for overlapping solutions, proposed by Belytschko and Xiao [7].

Remark 5
Problem described by Equation (17) can be solved over a smaller subdomain $\Omega_{\text{sub}} \subseteq \Omega$ by defining a representative domain or unit cell with periodic Neumann boundary conditions. Consequently, the cost of solving (17) around the point defects can be reduced substantially.

3. NANOSCALE PARAMETER-DEPENDENT MECHANICAL MATERIAL PROPERTIES OF NANOTUBES

In the quasi-continuum modeling of defect-free nanostructure facilitated by Equation (16), interatomic interactions are incorporated through nanoscale-based material moduli. These moduli are defined via internal variables that are functions of changes in bond lengths and bond angles and, therefore, depend on the local atomic configurations.

3.1. The molecular mechanics model

In general materials are modeled either via phenomenological/continuum models or via quantum/molecular mechanics models. The latter includes classical MD and *ab initio* methods. From a computational viewpoint, molecular mechanics and/or quantum mechanics models are

DOI: 10.1002/nme

expensive to be carried out on nanotubes where length is of the order of micrometers. On the other hand, continuum mechanics models do not take into account changes in structure at the molecular level of the materials and therefore cannot precisely model vacancy defects or Stone–Wales transformations.

From molecular mechanics perspective, the nanosystem energy can be written as

$$U = U_\rho + U_\theta + U_\varphi + U_\omega + U_{\text{vdw}} + U_{\text{es}} \tag{19}$$

where U_ρ is the bond stretch energy, U_θ is the energy due to bond angle bending, U_φ is the inversion energy, U_ω is the torsional energy, U_{vdw} represents the Van der Waals energy, and U_{es} is the electrostatic energy. For the axial deformations in graphene sheets and CNTs, a stick-spiral model wherein the system energy is based on nuclear positions has been presented by Chang and Gao [21]. We follow [21] and consider the bond stretch energy U_ρ and bond angle bending energy U_θ in the molecular mechanics model, and ignore the other energy contributions. Consequently, (19) is reduced to the following equation:

$$U(\Delta r, \Delta\theta) = U_\rho(\Delta r) + U_\theta(\Delta\theta) \tag{20}$$

The functional forms of the bond stretch energy and bond angle rotation energy that are considered in this work are given by the modified Morse potentials presented in [6] and are written as follows:

$$U_\rho(\Delta r) = D_e\{[1 - e^{-\beta\Delta r}]^2 - 1\} \tag{21}$$

$$U_\theta(\Delta\theta) = \tfrac{1}{2}K_\theta(\Delta\theta)^2[1 + K_{\text{sextic}}(\Delta\theta)^4] \tag{22}$$

where Δr and $\Delta\theta$ are the changes in the bond length and the bond angle, respectively. The various constants in Equations (21) and (22) are given in [6]: $D_e = 0.6031\,\text{nN nm}$, $K_{\text{sextic}} = 0.754\,\text{rad}^{-4}$, $\beta = 26.25\,\text{nm}^{-1}$, $K_\theta = 1.42\,\text{nN nm/rad}^2$.

By differentiating the energy equations (21) and (22) with respect to Δr and $\Delta\theta$, one obtains the force–stretch and moment angle–variation relations, respectively, as follows:

$$F(\Delta r) = 2\beta D_e(1 - \text{e}^{-\beta\Delta r})\text{e}^{-\beta\Delta r} \tag{23}$$

$$M(\Delta\theta) = k_\theta\Delta\theta[1 + 3k_{\text{sextic}}(\Delta\theta)^4] \tag{24}$$

Remark 6

One can consider other functional forms of the bond stretch energy and bond angle rotation energy (see, e.g. [11–15]) in the stick-spiral model that is used in conjunction with the multiscale framework proposed here.

3.2. The stick-spiral model

This section describes the stick-spiral model by Chang and Gao [21] that is derived based on the molecular mechanics model for CNTs. Employing kinematic considerations, this model provides relations between axial force f, axial-strain ε, and lateral strain ε' in terms of the changes in bond lengths and bond angles. We have employed this model to extract bond length and bond

DOI: 10.1002/nme

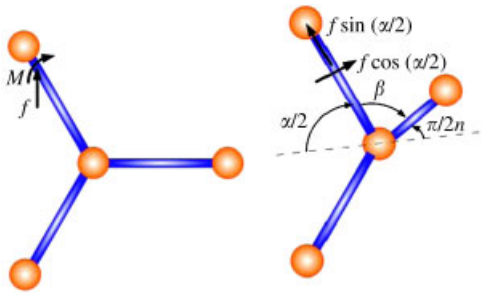

Figure 1. Schematic force and moment balance diagram for a typical pattern of four carbon atoms connected via three bond lengths. Localized strains are supposed to be homogeneous at a given point though they may change from point to point in the domain (see [21] for details).

angle-dependent mechanical material properties, where the changes in the bond lengths and bond angles are obtained from the converged strain fields during non-linear calculations of mechanically deforming nanotubes. For clarity of presentation, we briefly outline the salient features of the stick-spiral model, followed by the procedure how these nanoscale-based mechanical properties are employed in the proposed multiscale computational framework.

Figure 1 presents four carbon atoms that are connected via three interatomic bonds, i.e. a typical unit that repeats itself to yield hexagonal patterns in CNTs and produces graphene sheets in a planar configuration. From a kinematic viewpoint, an externally applied axial force f results in changes in the bond lengths and bond angles till the new stretched configuration comes in a state of self equilibrium. Our objective is to find these equilibrated bond lengths and angles, and we use the stick-spiral model of Chang and Gao [21] that provides a set of analytical equations that relate axial force with axial and lateral strain via the changes in bond lengths and bond angles.

3.2.1. Equilibrium relations. As shown in Figure 1, for any pair of carbon atoms, a component of force f acts along the line connecting the two atoms and a component is orthogonal to it. The force component that acts along the bond length results in stretching the bond and the component that is orthogonal results in changing the bond angle. On the basis of these kinematic considerations, Chang and Gao [21] present a stick-spiral model that gives force–equilibrium relations and the moment–equilibrium relations for the armchair nanotubes (n,n) and zigzag nanotubes $(n,0)$. For the sake of completeness of discussion, these relations are listed as follows:

Armchair nanotubes (n,n):

$$f\sin(\alpha/2) = F(\Delta r) \quad (\textit{Force equilibrium}) \tag{25}$$

$$f(r/2)\cos(\alpha/2) = M(\Delta\alpha) + M(\Delta\beta)\cos(\phi) \quad (\textit{Moment equilibrium}) \tag{26}$$

Zigzag nanotubes $(n,0)$:

$$f\cos(\pi-\alpha) = F(\Delta r) \quad (\textit{Force equilibrium}) \tag{27}$$

$$f(r/2)\sin(\pi-\alpha) = M(\Delta\alpha) + M(\Delta\beta)\cos(\phi) \quad (\textit{Moment equilibrium}) \tag{28}$$

DOI: 10.1002/nme

3.2.2. Kinematic relations. From the stick-spiral model for armchair and zigzag nanotubes the changes in bond length and bond angle are related to the axial strain via the following expressions:

Armchair nanotubes (n,n):

$$\varepsilon=[\Delta r\sin(\alpha/2)+(r/2)\cos(\alpha/2)\Delta\alpha]/[r\sin(\alpha/2)] \tag{29}$$

where $\alpha=2\pi/3$ and $\beta=\pi-\arccos[0.5\cos(\pi/(2n))]$.

Zigzag nanotubes $(n,0)$:

$$\varepsilon=[\Delta b+\Delta r\cos(\pi-\alpha)+r\sin(\pi-\alpha)\Delta\alpha]/[r[1+\cos(\pi-\alpha)]] \tag{30}$$

where $\alpha=2\pi/3$ and $\beta=\arccos[0.25-0.75\cos(\pi/n)]$ and Δb is the change in the bond length that is aligned with the direction of the axis of the zigzag nanotube. For the linear potential presented in Chang and Gao [21], $\Delta b=2\Delta r/\cos(\pi-\alpha)$.

3.3. Extracting the quasi-continuum mechanical properties for CNTs

Substituting the force–stretch relation (23) and moment angle–variation relation (24) in the force–equilibrium and moment–equilibrium relations from Section 3.2.1 we get two equations in terms of axial force f. Substituting for f from one into the other gives rise to one non-linear equation in terms of the changes in bond length Δr and bond angle $\Delta\theta$, which are still unknowns. In order to solve the two unknowns Δr and $\Delta\theta$, we need one more equation. This equation is provided by the kinematic relations in the stick-spiral model in terms of the given applied axial strain ε and the kinematic quantities Δr and $\Delta\theta$, as presented for the armchair and the zigzag nanotubes in Section 3.2.2. Now solving the two equations in a *self-consistent fashion* yields the equilibrated values for Δr and $\Delta\theta$. These values are then used to extract the quasi-continuum properties of the defect-free nanotubes as follows:

Armchair nanotubes (n,n):

Using Δr in the force–equilibrium relation (25) we get axial force f that yields axial stress σ defined as

$$\sigma=f/(rt[1+\cos(\alpha/2)]) \tag{31}$$

where $t=0.34\,\text{nm}$ is the interlayer spacing in graphite. The lateral strain ε' for the armchair CNTs is given by the stick-spiral model as:

$$\varepsilon'=(\Delta r\cos(\alpha/2)-r/2\sin(\alpha/2)\Delta\alpha)/(r[1+\cos(\alpha/2)]) \tag{32}$$

Zigzag nanotubes $(n,0)$:

Using Δr in the force–equilibrium relation (27) we get axial force f that yields axial stress σ defined as

$$\sigma=f/(rt\sin(\pi-\alpha)) \tag{33}$$

The lateral strain ε' for the zigzag CNTs is given by the stick-spiral model as:

$$\varepsilon'=(\Delta r\sin(\pi-\alpha)-r\cos(\pi-\alpha)\Delta\alpha)/(r\sin(\pi-\alpha)) \tag{34}$$

DOI: 10.1002/nme

Once the stress and lateral strain are evaluated via the stick-spiral model, the scale-dependent mechanical material properties of Young's modulus and the Poisson ratio are obtained as:

Young's modulus:

$$E = \sigma/\varepsilon \tag{35}$$

The Poisson's ratio:

$$v = -\varepsilon'/\varepsilon \tag{36}$$

Remark 7

The procedure presented above is repeated at every step and for every integration point in an element, and it results in continuous updating of the mechanical parameters that are then used in the quasi-continuum model given in Equation (16).

3.3.1. Procedural outline for extracting nanoscale-dependent properties. This section provides a summary of the procedure described in Sections 3.1–3.3. Once the converged displacement field is attained that yields converged strains, the next step is to extract the changes in bond lengths and bond angles corresponding to the new equilibrated state. The stick-spiral model of Chang and Gao [21] provides moment equilibrium and force equilibrium equations, and based on kinematic considerations it also provides a relation between the longitudinal strain and the changes in bond lengths and bond angles. We employ interatomic potentials in these equations and find the equilibrated bond lengths and bond angles. This is done as follows (say for the armchair nanotubes):

1. Substituting the force–stretch relation (23) and the moment angle–variation relation (24) in the force–equilibrium relation (25) and the moment–equilibrium relation (26) yields two equations in terms of axial-force/bond f. Eliminating f via substitution from one of these equations into another yields a non-linear relation between Δr and $\Delta\alpha$.
2. Kinematic considerations of the stick-spiral model of Chang and Gao [21] yield a relation between longitudinal strain ε, Δr and $\Delta\alpha$ as describe in Section 3.2.2.
3. Given the converged longitudinal strain obtained from the converged displacement fields in the non-linear calculations, one can solve the two equations in a self-consistent fashion and obtain the values of changes in bond lengths Δr and bond angles $\Delta\alpha$.
4. Once Δr and $\Delta\alpha$ are evaluated numerically, Equations (31)–(36) present the procedure to evaluate nanoscale-dependent mechanical properties of nanomaterials.
5. To economize the computations, the nanoscale-based elastic constants are evaluated only at the beginning of each load step because at that time level a converged strain field is available from previous load step.

Remark 8

The case of graphene sheet is attained in the limit as $n \to \infty$ and the angles are $\alpha = \beta = 2\pi/3$. We follow the procedure outlined above to extract the scale-dependent mechanical material properties that are then used in the quasi-continuum modeling of the continuously deforming graphene sheets.

DOI: 10.1002/nme

4. A FRAMEWORK FOR MODELING POINT DEFECTS IN NANOTUBES

This section provides physical meanings to the additive split of the forcing function $\mathbf{f}$ that was introduced in Section 2. We consider $\tilde{\mathbf{f}}$ as the force field for the quasi-continuum model used for the defect-free nanotubes and graphene sheets where the modulus of elasticity E and the Poisson's ratio v are calculated based on nanoscale parameters presented in Section 3. In order to apply the multiscale framework to the modeling of point defects in nanotubes and graphene sheets, we need to provide physical meanings to the term $\mathbf{f}'$ and then describe a method to derive $\mathbf{f}'$.

Localized defects appear in the form of pentagons or heptagons embedded in regular hexagonal pattern in CNTs and graphene sheets. The local bond lengths and bond angles around defects are therefore different from that in the defect-free region in its ground state. Consequently, the localized energy around the defects is higher as compared with the energy in the defect-free region. In our multiscale framework presented in (9), $\mathbf{f}'$ represents the force field corresponding to the excess localized energy around the defect that helps in maintaining the surrounding atoms in their new equilibrated state with associated bond lengths and bond angles. This fine-scale force field $\mathbf{f}'$ is employed in Equation (11) to model the mechanical fields in the vicinity of the defects.

4.1. Formation energy of vacancy

This section presents procedure for evaluation of formation energy of defect. Figure 2 shows a schematic diagram of atoms and the bonds affected by the presence of vacancy. In our calculations we have assumed that only immediate neighboring atoms, as indicated in blue color in Figure 2, are affected by the presence of divacancy. We have employed second generation Brenner potentials for calculations of defect formation energy [15]. The assumption of using only the immediate neighboring atoms in the evaluation of formation energy is reasonable when one observes that Brenner potential has a cut off of 0.2 nm, while the bond length is 0.142 nm for unstrained nanotube. This defines the patch of atoms that contribute to the formation energy of vacancy. The size of the computational cell, which in the context of the finite element method is the element that contains the defect, can be of the order of five–ten times the patch size. Suppose there are 'N' carbon atoms

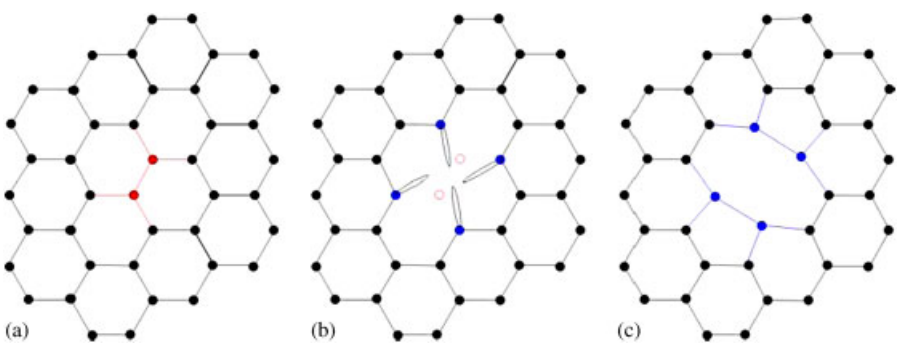

Figure 2. Relaxation of atoms around the defect: (a) hexagonal pattern without defect, divacancy sites shown in red; (b) configuration of atoms with divacancy and dangling bonds. Immediate neighboring atoms, shown in blue, are allowed to relax; and (c) relaxation and reconfiguration of atoms around divacancy.

DOI: 10.1002/nme

in the non-defective patch. We can evaluate the average stretch energy stored in a carbon–carbon bond of this system as described below.

The total energy of perfect lattice as shown in Figure 2(a) is evaluated as follows:

$$E_{\text{non-defective}} = \frac{1}{2} \sum_{i,j\,(i \neq j)}^{N} [V^{\text{R}}(r_{ij}) - b_{ij} V^{\text{A}}(r_{ij})] \tag{37}$$

The functions $V^{\text{R}}(r_{ij})$ and $V^{\text{A}}(r_{ij})$ represent all interatomic repulsions and attractions from valence electrons, respectively, and are defined in Brenner *et al.* [15]. N is the number of atoms in the perfect lattice. The total energy of the lattice with divacancy is evaluated by allowing neighboring atoms around vacancy to relax. This is achieved through minimization of energy of this lattice with respect to varying lattice positions of immediate neighboring atoms. Figures 2(b) and (c) show the relaxation and reconfiguration of atoms around divacancy.

The formation energy is defined as follows:

$$E_{\text{vacancy}}^{\text{formation}} = E_{\text{defective}}^{\text{relaxed}} - \frac{N-2}{N} E_{\text{non-defective}} \tag{38}$$

where $E_{\text{defective}}^{\text{relaxed}}$ is the total energy of the defective lattice after allowing relaxation of neighboring atoms. The average stretch energy in defective lattice is obtained as

$$U_{\rho}^{\text{defective}} = U_{\rho}^{\text{non-defective}}(\Delta r) + \frac{E_{\text{vacancy}}^{\text{formation}}}{M} \tag{39}$$

where M is the total number of bonds in the defective lattice.

We reconsider (20) and modify the stretch energy of the defect-free material with the energy given by (39). Taking derivative with respect to the change in bond length Δr we get an expression for the homogenized force–stretch relation:

$$\begin{aligned} F(\Delta r)_{\text{defective}} &= \partial U_{\rho}^{\text{defective}} / \partial \Delta r \\ &= F(\Delta r) + \frac{F_{\text{formation}}}{M} \end{aligned} \tag{40}$$

where

$$\begin{aligned} F_{\text{formation}} &= \partial E_{\text{vacancy}}^{\text{formation}} / \partial \Delta r \\ &= \partial E_{\text{defective}}^{\text{relaxed}} / \partial \Delta r - \frac{(N-2)}{N} (\partial E_{\text{non-defective}} / \partial \Delta r) \end{aligned} \tag{41}$$

Once the updated force–stretch relation is obtained via (40), we employ the procedure outlined in Section 3 to extract the nanoscale-based quasi-continuum mechanical material properties around the point defects in the nanotubes. These material parameters are then used in the variational problem driven by $\mathbf{f}'$.

Remark 9

In order to keep the model and associated calculations simple, the defect is assumed to be frozen during the course of deformation of CNTs, i.e. neither do further interatomic bonds appear nor do the existing bonds break at or around the current defect.

DOI: 10.1002/nme

Remark 10
It is important to note that the scale-dependent nanomechanical material properties are evaluated based on the new equilibrated bond lengths and bond angles around the point defect. These values are different from the equilibrated bond lengths and angles away from the defect.

Remark 11
Similar computations can be made for defects like Stone–Wales transformations. Zhou and Shi [24] give a simple empirical formula to evaluate Stone–Wales formation energy in case of carbon nanotubes. Li *et al*. [25] have computed formation energies of Stone–Wales defect through first principle methods in case of graphite. The computed formation energy can be used to extract material properties as outlined in the procedure described above.

4.2. Evaluation of the force component $\mathbf{f}'$

In the multiscale framework presented in Equation (9), $\mathbf{f}'$ represents the force field corresponding to the excess localized energy around the defect that maintains the surrounding atoms in their new equilibrated state with new bond lengths and bond angles as shown in Figure 2. We write the minimization problem of the relative energy in a weak form and the fine-scale force field $\mathbf{f}'$ is extracted by solving a linearized variational equation at each load step.

$$(w_i, f_i') = (w_{i,j}, \sigma_{ij}^{\text{defective}}) - (w_{i,j}, \sigma_{ij}^{\text{non-defective}}) \tag{42}$$

where $\boldsymbol{\sigma}^{\text{defective}}$ represents the stress field of the defective patch and $\boldsymbol{\sigma}^{\text{non-defective}}$ represents the stress field associated with the non-defective patch. Figure 3 shows the schematic diagram of the finite element mesh indicating the coarse element that contains the defect. A sub-mesh is generated over this coarse mesh as shown in Figure 3 and the sub intervals of this refined mesh are termed as computational cells.

Weak solution to Equation (42) in the computational cell containing defect yields $\mathbf{f}'$. The contribution to $\mathbf{f}'$ from other cells in the sub-mesh is zero because these cells do not contain the defect. It is reasonable to assume that the effect of $\mathbf{f}'$ is localized around the point defect. Consequently Equation (17) is solved on the refined sub-mesh that is generated over the element of the coarse mesh containing the point defect, and is termed as the super-element (see Figure 3).

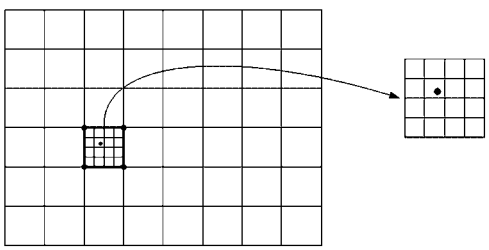

Figure 3. Schematic diagram of finite element mesh indicating the element that possesses the defective patch. Computational cell is defined as a subinterval of the refined mesh that overlays the element containing defect. In this context element of the coarse mesh that contains defect becomes a super-element. Point defect in the cell is indicated by the dot.

DOI: 10.1002/nme

4.3. Salient features of the formulation for modeling defects in nanostructures

1. The quasi-continuum model has nanolength-scales built in it because of the dependence of the modulus of elasticity $E(\Delta r, \Delta\theta)$ and the Poisson's ratio $v(\Delta r, \Delta\theta)$ on the changes in the interatomic bond lengths Δr and bond angles $\Delta\theta$.
2. The local defects in the graphene sheet induce an atomic-scale (fine scale) force field, which is indicated by $\mathbf{f}'$. This atomic-scale force field is obtained through Equation (42) where formation energy of the vacancy embedded with interatomic potentials for defective and non-defective nanostructure has been employed to define $\boldsymbol{\sigma}^{\text{defective}}$ and $\boldsymbol{\sigma}^{\text{non-defective}}$. This fine-scale force field drives the problem for the localized displacement field around defects in the nanostructure.
3. The case where problems driven by $\tilde{\mathbf{f}}$ and $\mathbf{f}'$ given in Equations (16) and (17), respectively, are linear problems, the total solution around defects can be obtained via principle of superposition as

$$\tilde{\mathbf{u}} = \tilde{\mathbf{u}}_{\tilde{\mathbf{f}}} + \tilde{\mathbf{u}}_{\mathbf{f}'} \tag{43}$$

4. The case where problems driven by $\tilde{\mathbf{f}}$ and $\mathbf{f}'$ are non-linear, Lagrange multiplier methods for overlapping solutions can be employed as presented in Belytschko and Xiao [7].
5. The case where body force $\tilde{\mathbf{f}} = \mathbf{0}$, the problem for the defect-free nanostructure (graphene sheet or nanotubes) is driven by edge traction and/or the prescribed edge displacement fields.
6. The defective inter-atomic bond lengths are on the order of nanometers (see Figure 2). The defective patch of atoms that contains the point defect and is used to evaluate energy associated with $\mathbf{f}'$ via (39)–(41) is typically spread over six–eight bond diameters. The size of the computational cell (i.e. sub-interval of the sub-mesh) can be taken equal to five–ten times the patch size (see Figure 3). Employing a refined sub-mesh, the super-element that contains the cells can be one–two orders of magnitude larger than the representative computational cell that contains the point defect. Depending on the size of the global mesh, which can be another one–two orders of magnitude larger than the element on which the refined sub-mesh is created, one can scale up from the nanometer 10^{-9} m range to a specimen size that lies between microscale 10^{-6} m and mesoscale 10^{-4} m.
7. Defects in the nanostructure are explicitly represented via the interatomic potentials. For the case when there are no defects in the lattice, $\mathbf{f}' = \mathbf{0}$ and the solution given by $\tilde{\mathbf{u}}_{\tilde{\mathbf{f}}}$ is the total solution for the defect-free nanostructure. This is a very important attribute of the proposed computational framework and ensures that the proposed method is a self-consistent method.

5. NUMERICAL RESULTS

The multiscale framework presented in Section 2 leads to a hierarchical finite element method that has been implemented using four-node isoparametric elements [26, 27]. As presented in Section 3, the mechanical material properties are evaluated at the integration points via a set of internal variables that are functions of interatomic potentials. These interatomic potentials are functions of the changes in the bond lengths and bond angles that occur because of the local state of deformation. The underlying idea is based on internal variable formalism for the nanoscale-based mechanical material properties and a consistent updating of material properties that concurrently feeds information from the molecular scales into the quasi-continuum equations. The resulting

DOI: 10.1002/nme

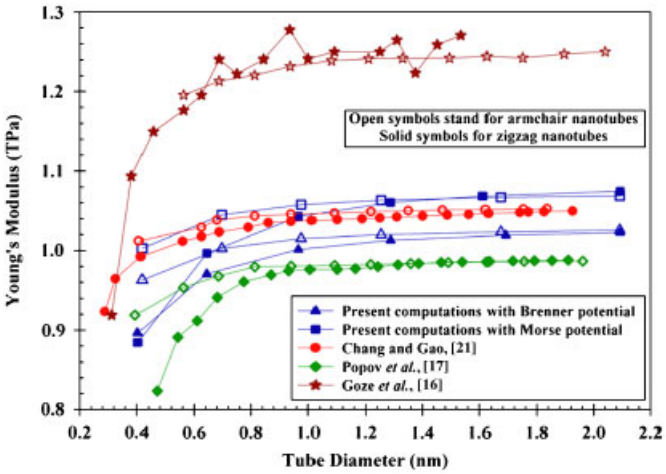

Figure 4. Young's modulus for non-defective nanotubes.

non-linear finite element method is used for studying the mechanical response of defect-free and defective CNTs.

5.1. Mechanical response of defect-free nanotubes

This section presents the simulated mechanical material properties of zigzag and armchair tubes. Two types of interatomic potentials have been investigated by incorporating them in the nanostructural model: modified Morse potential [6] and the Tersoff–Brenner potential [15].

Figure 4 presents Young's modulus for the nanotubes as a function of the changes in the tube diameter. Open symbols represent the response of armchair nanotubes and solid symbols represent the response of zigzag nanotubes. Both modified Morse as well as the Brenner potentials have been employed to extract the modulus of elasticity of CNTs. The value of Young's modulus as predicted by using Brenner potential is approximately 5% higher than that predicted by Morse potential. For each of these cases the simulated Young's modulus is slightly higher for the armchair CNTs than that for the zigzag CNTs of the same diameter. Computed results are also compared with published literature where results from [16] are an upper bound and results from [17] are a lower bound to the present calculations. The predicted mechanical response lies in the general range of the expected mechanical material properties for the various types of CNTs [29, 30].

Figure 5 presents the Poisson ratio for the two types of nanotubes as a function of change in the tube diameter. Once again modified Morse as well as the Brenner potentials have been employed and a good agreement has been attained with the published results.

5.2. Mechanical response of nanotubes with topographical defects

The proposed multiscale framework is also applied to the modeling of mechanical response of CNTs with topographical defects such as vacancies (see, e.g. [6, 24, 31]). We consider that the defects arise because of missing atoms that result in a change in the hexagonal pattern in graphene sheets and nanotubes. These defects stay frozen during the mechanical loading of the CNT, i.e. further defects do not appear as a function of deformation. Figure 6 shows a schematic diagram of

DOI: 10.1002/nme

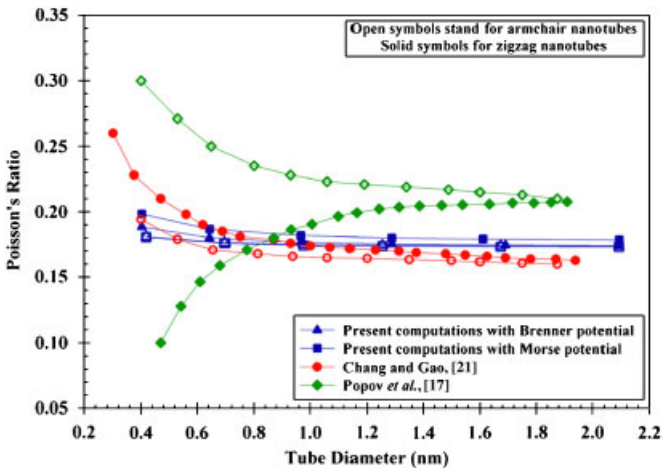

Figure 5. Poisson's ratio for non-defective nanotubes.

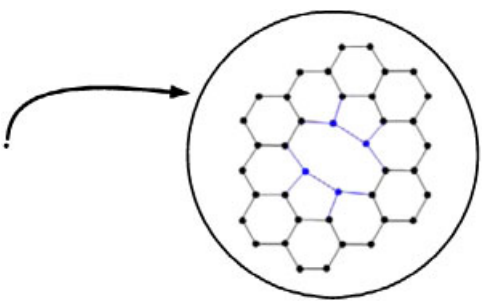

Figure 6. A schematic diagram of divacancy defect.

a defect due to divacancy that is assumed to exist in the initial configuration of the CNT and this defect persists through the deformation process. Figures 7 and 8 present the stress–strain plots for the non-defective and defective (5,5) armchair tubes, respectively. Once again results are compared with various theoretical models presented in [31], primarily based on quantum mechanics and molecular dynamics models. The present model predicts the nano-stress–strain relation with great accuracy. It is important to note that these results have been obtained on a single processor desktop computer at a fraction of the computational effort as compared with the quantum mechanics and molecular dynamics models.

Figures 9 and 10 present Young's modulus as a function of increasing deformation represented in the form of increasing strain for the non-defective and defective (5,5) armchair CNTs. These calculations were also carried out on a single processor desktop computer. Once again the multiscale model predicts mechanical properties within the envelope provided by the DFT and the PM3 models reported in [31].

DOI: 10.1002/nme

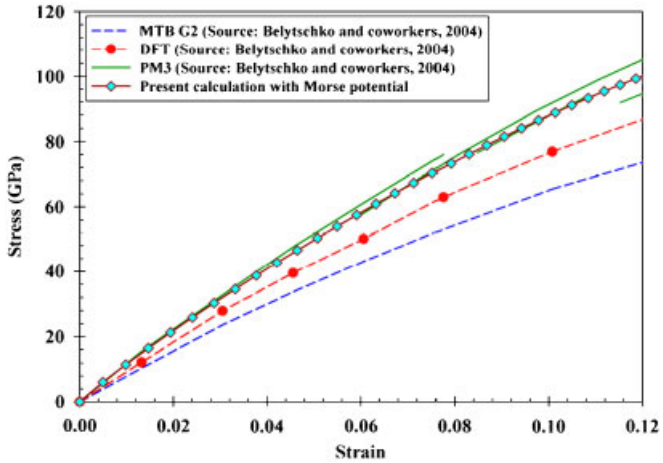

Figure 7. Stress–strain response of non-defective nanotube (see Reference [31]).

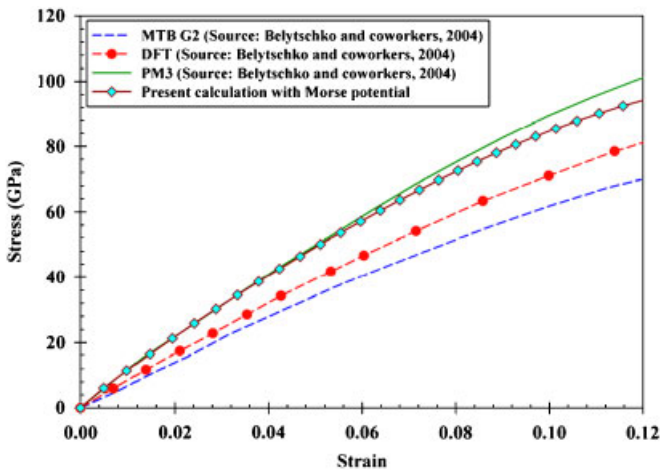

Figure 8. Stress–strain response of defective nanotube (see Reference [31]).

6. CONCLUDING REMARKS

We have presented a hierarchical multiscale computational framework for bridging the gap between molecular mechanics at nanoscales and quasi-continuum mechanics at microscales in the modeling of CNTs. The proposed two-level scale separation results in a coupled self-consistent system of equations, which is then systematically decoupled to yield a set of equations for modeling defect-free CNTs, and a second set for modeling the defects in CNTs. The ensuing finite element method also furnishes two-level statement of the problem, with level-one providing a method for modeling defect-free nanostructure and level-two providing a method for modeling defects

DOI: 10.1002/nme

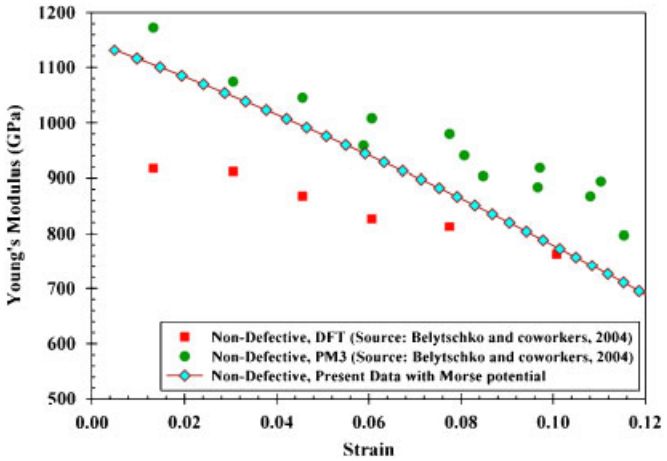

Figure 9. Young's modulus as function of strain for non-defective nanotubes (see Reference [31]).

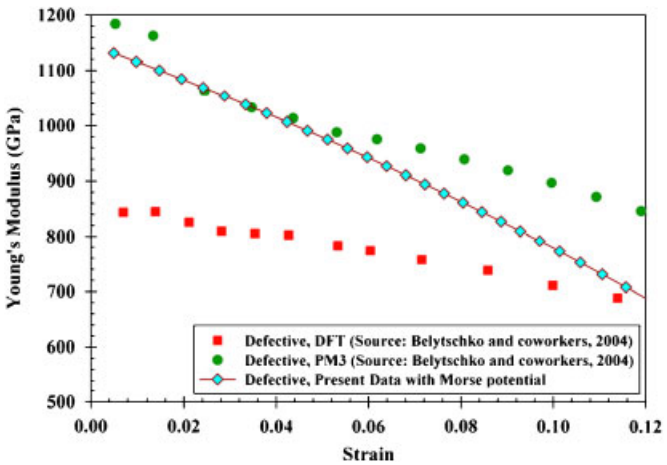

Figure 10. The Poisson's ratio as function of strain for defective nanotubes (see Reference [31]).

in the nanostructure. In the quasi-continuum model, interatomic interactions are incorporated via nanoscale material moduli that are based on interatomic potentials, which are in turn functions of the local state of deformation. Two types of interatomic potentials, i.e. modified Morse potentials and the Tersoff–Brenner potentials are employed in the evaluation of nanoscale material moduli. The concept of formation energy of vacancy is employed to extract the fine-scale force fields that are then used in the level-two finite element discretization to model defects. Point defects that arise because of vacancies and affect atomic structure locally are discretely modeled. Representative numerical examples are shown to validate the model and demonstrate its range of applicability.

DOI: 10.1002/nme

ACKNOWLEDGEMENTS

This work was partially supported by Office of Naval Research Grant N000014-02-1-0143, and the National Academy of Sciences Grant NAS 7251-05-005. This support is gratefully acknowledged.

REFERENCES

1. Iijima S. Helical microtubes of graphitic carbon. *Nature* 1991; **354**:56–58.
2. Maiti A. Carbon nanotubes: bandgap engineering with strain. *Nature Materials* 2003; **2**:440–442.
3. Pitkethly MJ. Nanomaterials—the driving force. *Materials Today* 2004; **7**(12, Suppl. 1):20–29.
4. Qian D, Wagner GJ, Liu WK, Yu M, Ruoff RS. Mechanics of carbon nanotubes. *Applied Mechanics Reviews* 2002; **55**(6):495–553.
5. Liu WK, Karpov EG, Zhang S, Park HS. An introduction to computational nanomechanics and materials. *Computer Methods in Applied Mechanics and Engineering* 2004; **193**:1529–1578.
6. Belytschko T, Xiao SP, Schatz GC, Ruoff RS. Atomistic simulations of nanotube fracture. *Physical Review B* 2002; **65**:235–430.
7. Belytschko T, Xiao SP. Coupling methods for continuum model with molecular model. *International Journal for Multiscale Computational Engineering* 2003; **1**(1):115–126.
8. Arroyo M, Belytschko T. Continuum mechanics modeling and simulation of carbon nanotubes. *Mechanica* 2005; **40**:455–469.
9. Yakobson BI, Brabec CJ, Bernholc J. Nanomechanics of carbon tubes: instabilities beyond linear response. *Physical Review Letters* 1996; **76**:2511–2514.
10. Buongiorno-Nardelli M, Yakobson BI, Bernhold J. Brittle and ductile behavior in carbon nanotubes. *Physical Review Letters* 1998; **81**:4656–4659.
11. Morse PM. Diatomic molecules according to the wave mechanics. II. Vibrational levels. *Physical Review* 1929; **34**:57–64.
12. Tersoff J. Empirical interatomic potential for carbon, with applications to amorphous-carbon. *Physical Review Letters* 1988; **61**:2872–2879.
13. Tersoff J. Empirical interatomic potential for carbon, with applications to amorphous carbon. *Physical Review Letters* 1988; **61**(25):2879–2882.
14. Brenner DW. Empirical potential for hydrocarbons for use in simulating the chemical vapor-deposition of diamond films. *Physical Review B* 1990; **42**:9458–9471.
15. Brenner DW, Shendevora OA, Harrison JA, Stuart SJ, Ni B, Sinnott SB. A second-generation reactive empirical bond orders (REBO) potential energy expression for hydrocarbons. *Journal of Physics*: *Condensed Matter* 2002; **14**:783–802.
16. Goze C, Vaccarini L, Henrard L, Bernier P, Hernandez E, Rubio A. Elastic and mechanical properties of carbon nanotubes. *Synthetic Metals* 1999; **103**:2500–2501.
17. Popov VN, Van Doren VE, Balkanski M. Elastic properties of single-walled carbon nanotubes. *Physical Review B* 2000; **61**:3078–3084.
18. Zhang S, Khare R, Lu Q, Belytschko T. A bridging domain and strain computation method for coupled atomistic–continuum modelling of solids. *International Journal for Numerical Methods in Engineering* 2007; **70**:913–933.
19. Zhang P, Huang Y, Geubelle PH, Hwang KC. On the continuum modeling of carbon nanotubes. *Acta Mechanica Sinica* 2002; **18**:528–536.
20. Zhang P, Huang Y, Geubelle PH, Klein PA, Hwang KC. The elastic modulus of single-wall carbon nanotubes: a continuum analysis incorporating interatomic potentials. *International Journal of Solids and Structures* 2002; **39**:3893–3906.
21. Chang T, Gao H. Size-dependent elastic properties of a single-walled carbon nanotube via a molecular mechanics model. *Journal of the Mechanics and Physics of Solids* 2003; **51**:1059–1074.
22. Chong KP. Nanoscience and engineering in mechanics and materials. *Journal of Physics and Chemistry of Solids* 2004; **65**:1501–1506.
23. Liu B, Jiang H, Huang Y, Qu S, Yu M-F, Kwang KC. Atomic-scale finite element method in multiscale computation with applications to carbon nanotubes. *Physical Review B* 2005; **72**:035435.
24. Zhou LG, Shi SQ. Formation energy of Stone–Wales defects in carbon nanotubes. *Applied Physics Letters* 2003; **83**(6):1222–1224.

DOI: 10.1002/nme

25. Li L, Reich S, Robertson J. Defect energies of graphite: density-functional calculations. *Physical Review B* 2005; **72**:184109.
26. Masud A, Kannan R, Xia K. A multiscale framework for computational nanomechanics: application to carbon nanotubes. *Proceedings of the 5th International Conference on Computation of Shell and Spatial Structures*, Ramm E, Wall WA, Bletzinger K-U, Bischoff M (eds). Salzburg, Austria, 1–4 June 2005.
27. Masud A, Kannan R. A multiscale computational framework for the modeling of carbon nanotubes. In *Proceedings of the VIII International Conference on Computational Plasticity* (*COMPLAS VIII*), Onate E, Owen DRJ (eds). CIMNE Barcelona, Spain, 5–8 September 2005.
28. Masud A, Franca LP. A hierarchical multiscale framework for problems with multiscale source terms. *Computer Methods in Applied Mechanics and Engineering* 2008; **197**:2692–2700.
29. Xiao JR, Gama BA, Gillespie Jr JW. An analytical molecular structural mechanics model for the mechanical properties of carbon nanotubes. *International Journal of Solids and Structures* 2005; **42**:3075–3092.
30. Jiang H, Zhang P, Liu B, Huang Y, Guebelle PH, Gao H, Hwang KC. The effect of nanotube radius on the constitutive model for carbon nanotubes. *Computational Materials Science* 2003; **28**:429–442.
31. Mielke SL, Troya D, Zhang S, Li J, Xiao S, Car R, Ruoff RS, Schatz GC, Belytschko T. The role of vacancy defects and holes in the fracture of carbon nanotubes. *Chemical Physics Letters* 2004; **390**:413–420.

DOI: 10.1002/nme